ISSN 0021-3640, JETP Letters, 2023, Vol. 118, No. 9, pp. 676–683. © The Author(s), 2023. This article is an open access publication.
Russian Text © The Author(s), 2023, published in Pis'ma v Zhurnal Eksperimental'noi i Teoreticheskoi Fiziki, 2023, Vol. 118, No. 9, pp. 689–696.

CONDENSED MATTER

Metal–Insulator Transition and Other Electronic Properties of AB-Stacked Bilayer Graphene Deposited on a Ferromagnetic Substrate

I. E. Gobelko[a], A. V. Rozhkov[b, *], and D. N. Dresvyankin[c]

[a] *Moscow Institute of Physics and Technology (National Research University), Dolgoprudnyi, Moscow region, 141700 Russia*

[b] *Institute for Theoretical and Applied Electrodynamics, Russian Academy of Sciences, Moscow, 125412 Russia*

[c] *Skolkovo Institute of Science and Technology, Moscow, 121205 Russia*

** e-mail: arozhkov@gmail.com*

Received September 20, 2023; revised October 5, 2023; accepted October 6, 2023

Using a simple theoretical model, AB-stacked bilayer graphene deposited on a ferromagnetic insulating substrate is studied. In addition to the exchange Zeeman field induced by the substrate, the model allows one to take into account the effective external electric field perpendicular to the graphene sample plane (such field arises due to the contact with the substrate and can also be induced by applying a gate voltage). It has been demonstrated that AB-stacked graphene in zero electric field is in a metallic state. As the field increases, a transition to the insulating phase occurs. The spectrum of electron states, the band gap, and other characteristics of the phases on both sides of the metal–insulator transition have been calculated. Our results are consistent with density functional theory calculations and can be useful for spintronics.

DOI: 10.1134/S0021364023603068

1. INTRODUCTION

Graphene and related materials are promising for applications in spintronics [1–3]. The main object of study in this work is the Bernal-stacked bilayer graphene (also referred to as AB-stacked graphene) [4–6], deposited on a ferromagnetic substrate. Such heterostructures are of interest because they allow a strong Zeeman exchange field, thus affecting the spin characteristics of the electron liquid in a graphene sample.

In recent years, active experimental and theoretical studies in this research field are underway. For example, the authors of experimental work [7] reported that insulating EuS magnetic substrates can induce exchange fields up to hundreds of tesla in a single-layer graphene sample. (Although dc magnetic fields generated in laboratories do not exceed several tens of tesla, the situation with high exchange fields is less problematic.) The authors of [7] observed the splitting of electron energy bands in the graphene sample, the transition of the electron liquid to a ferromagnetic state characterized by the quantum transport of spin-polarized charge carriers, and the spin Hall effect. The authors of theoretical works [8, 9] considered similar systems of bilayer graphene placed on insulating magnetic substrates made of different materials. In each case, the electron spectrum is determined by density functional theory calculations.

Numerical calculations are important for materials research. However, many properties of carbon systems can be described using single-electron models that allow analytical or semi-analytical solutions. In this work, we employ this approach to study AB-stacked bilayer graphene deposited on a ferromagnetic insulating substrate in the external electric field. Our model Hamiltonian generalizes that previously formulated in [10]. We explicitly determine single-electron spectra of AB-stacked graphene and study the magnetic and transport characteristics of the sample. In particular, we theoretically demonstrate that bilayer graphene can be in both insulating and metallic states depending on the relation between the exchange Zeeman and normal electric fields. Therefore, by varying the gate voltage, it is possible to control spin and charge transport in bilayer graphene. This possibility may be of interest for spintronics applications.

Our work is organized as follows. In Section 2, we formulate the model and study its simplest properties. The metal–insulator transition is discussed in Section 3. In Section 4, we compare the results of our calculations with the numerical data. We discuss our results and present conclusions in Section 5.

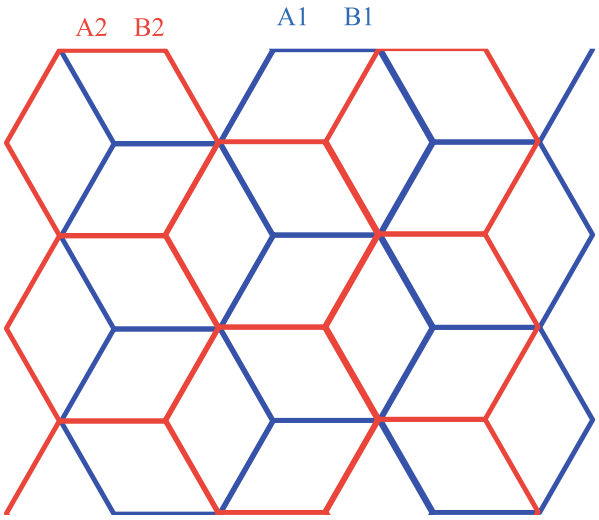

Fig. 1. (Color online) Crystal lattice of AB-stacked bilayer graphene, top view. The bottom and top layers are shown in blue and red, respectively. The four sublattices are denoted as A1, B1, A2, and B2.

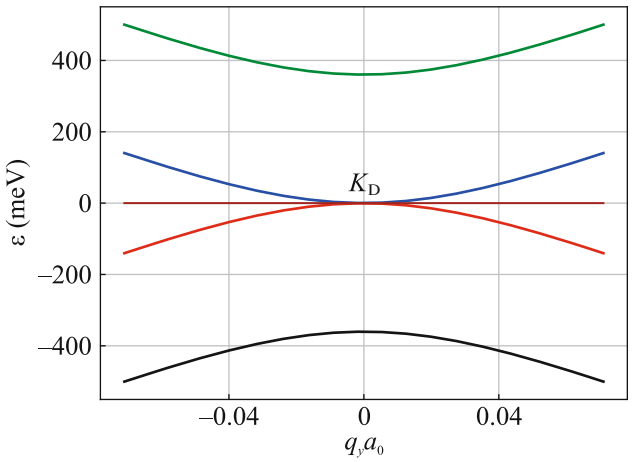

Fig. 2. (Color online) Dispersion curve of AB bilayer graphene (the $q_x = 0$ cut; q_y varies within a narrow range near the Dirac point K_D corresponding to $q_x = q_y = 0$). The horizontal line indicates the Fermi level $\varepsilon_F = 0$.

2. MODEL

AB-stacked bilayer graphene can be represented as two graphene sheets that are separated by a distance of $d = 0.36$ nm and are displaced with respect to each other by the carbon–carbon bond length $a_0 = 0.142$ nm, see Fig. 1. In such a lattice, each unit cell contains four carbon atoms, each of them belongs to one of four sublattices (A1 and B1 sublattices in the bottom layer and A2 and B2 sublattices in the top layer).

To describe an electron having the crystal momentum $\mathbf{q}$ at such a lattice, it is necessary to introduce four components of the wavefunction $\Psi_{\mathbf{q}}^{A1}$, $\Psi_{\mathbf{q}}^{B1}$, $\Psi_{\mathbf{q}}^{A2}$, and $\Psi_{\mathbf{q}}^{B2}$. It is convenient to compose them into the bispinor

$$\Psi_{\mathbf{q}} = (\Psi_{\mathbf{q}}^{A1}, \Psi_{\mathbf{q}}^{B1}, \Psi_{\mathbf{q}}^{A2}, \Psi_{\mathbf{q}}^{B2})^T. \quad (1)$$

Then, the Schrödinger equation can be written as

$$H_{\mathbf{q}}\Psi_{\mathbf{q}} = \varepsilon_{\mathbf{q}}\Psi_{\mathbf{q}}, \quad (2)$$

where $\varepsilon_{\mathbf{q}}$ is the eigenvalue, i.e., the energy, and the matrix $H_{\mathbf{q}}$

$$H_{\mathbf{q}} = \begin{pmatrix} 0 & -tf_{\mathbf{q}} & 0 & 0 \\ -tf_{\mathbf{q}}^* & 0 & -t_0 & 0 \\ 0 & -t_0 & 0 & -tf_{\mathbf{q}} \\ 0 & 0 & -tf_{\mathbf{q}}^* & 0 \end{pmatrix}, \quad (3)$$

plays the role of the Hamiltonian for the states with the crystal momentum $\mathbf{q}$. Here, $t = 2.57$ eV is the hopping amplitude between atoms in one layer, $t_0 = 0.36$ eV is the interlayer hopping amplitude, and $f_{\mathbf{q}} = 1 + 2\exp\left(\frac{3ia_0q_x}{2}\right)\cos\left(\frac{\sqrt{3}a_0q_y}{2}\right)$, where $\mathbf{q}$ is the crystal momentum measured from the Brillouin zone center. The eigenvalues $\varepsilon_{\mathbf{q}}$ are determined by the well-known formula

$$\varepsilon_{\mathbf{q}}^{(1,\ldots,4)} = \pm\frac{t_0}{2} \pm \sqrt{t^2|f_{\mathbf{q}}|^2 + \frac{t_0^2}{4}}. \quad (4)$$

Near the Dirac points $K_D = \left(0, \frac{4\pi}{3\sqrt{3}a_0}\right)$ and $K_D' = \left(0, -\frac{4\pi}{3\sqrt{3}a_0}\right)$, energy bands (4) are plotted in Fig 2. In zero applied field, AB-stacked graphene is in a semimetallic state: two lower bands are completely filled with electrons, whereas two upper bands are empty, the Fermi energy equals zero, $\varepsilon_F = 0$, and at the Dirac point, the empty and filled bands touch each other.

To take into account the effect of the magnetic substrate, we assume that the exchange Zeeman field induced by the substrate affects two layers differently. Namely, we refine the system of equations (2) as follows

$$(H_{\mathbf{q}} + V_\sigma)\Psi_{\mathbf{q}} = \varepsilon_{\mathbf{q}}\Psi_{\mathbf{q}}, \quad (5)$$

where

$$V_\sigma = \mathrm{diag}(\sigma h, \sigma h, \sigma\tilde{h}, \sigma\tilde{h}). \quad (6)$$

In this expression, h and $\tilde{h}$ are the Zeeman exchange energies in the top and bottom layers, respectively. Below, we always assume that $0 \le \tilde{h} \le h$; i.e., the exchange field in the layer being in the direct contact with the substrate is always higher than that in the layer not touching the substrate. (We express the numerical values of exchange fields in both electronvolts and teslas, the relation between these units is determined by the Bohr magneton $\mu_B \approx 5.79 \times 10^{-5}$ eV/T.)

The eight eigenvalues (four per each spin projection) of the set of equations (5) can be expressed by the single formula

$$\varepsilon_{\mathbf{q}\sigma}^{(1,\ldots,8)} = \frac{\sigma(h+\tilde{h})}{2} + \chi\left[\frac{(h-\tilde{h})^2}{4} + |f_{\mathbf{q}}|^2 t^2 + \frac{t_0^2}{2} + \kappa\sqrt{(h-\tilde{h})^2|f_{\mathbf{q}}|^2 t^2 + |f_{\mathbf{q}}|^2 t^2 t_0^2 + \frac{t_0^4}{4}}\right]^{1/2}. \quad (7)$$

Here, $\sigma = \pm 1$ is the projection of electron spin on the substrate magnetization vector, $\chi = \pm 1$, and $\kappa = \pm 1$. In the physically justified limit, $h \ll t_0 \ll t$, the energy of the states with $\chi = +1$ ($\chi = -1$) is positive (negative), except maybe a small neighborhood of the Dirac points.

Let the two bands closest to the Fermi level be labeled as 4 and 5 and bands 4, 5, 3, and 6 correspond to the following values of the parameters introduced in Eq. (7): $\sigma = +1$, $\chi = -1$, and $\kappa = -1$; $\sigma = -1$, $\chi = +1$, and $\kappa = -1$; $\sigma = -1$, $\chi = -1$, and $\kappa = -1$; and $\sigma = +1$, $\chi = +1$, and $\kappa = -1$, respectively.

The remaining bands 1, 2, 7, and 8 correspond to $\kappa = +1$. It is easy to check that $\min_{\mathbf{q}} |\varepsilon_F - \varepsilon_{\mathbf{q}}^{(1,2,7,8)}| \sim t_0$; i.e., these bands are located quite far from the Fermi level. Consequently, we can ignore them.

Expression (7) implies that

$$\varepsilon_{\mathbf{q}}^{(4)} = -\varepsilon_{\mathbf{q}}^{(5)}, \quad \varepsilon_{\mathbf{q}}^{(3)} = -\varepsilon_{\mathbf{q}}^{(6)}. \quad (8)$$

Hence, we see that the Fermi level in AB-stacked graphene corresponds to zero energy: $\varepsilon_{\mathbf{q}}^{(4)} = \varepsilon_{\mathbf{q}}^{(5)} = 0$ $\varepsilon_F = 0$. It is easy to check that bands 3 and 6 do not reach ε_F, whereas bands 4 and 5 overlap near the Dirac points, see Fig. 3. Such overlapping leads to the redistribution of charge carriers among the bands, which is accompanied by the formation of the electron and hole sheets of the Fermi surface. In other words, bilayer AB-stacked graphene at a nonzero exchange field h becomes metallic even without doping.

The Fermi surface formed due to the redistribution of charge carriers between bands 4 and 5 should be determined by solving the equation. This condition defines a doubly connected Fermi surface $\mathbf{q}_F$ in the crystal momentum space. Symmetry conditions (8) guarantee that the electron and hole sheets of the Fermi surface coincide with each other; i.e., nesting occurs.

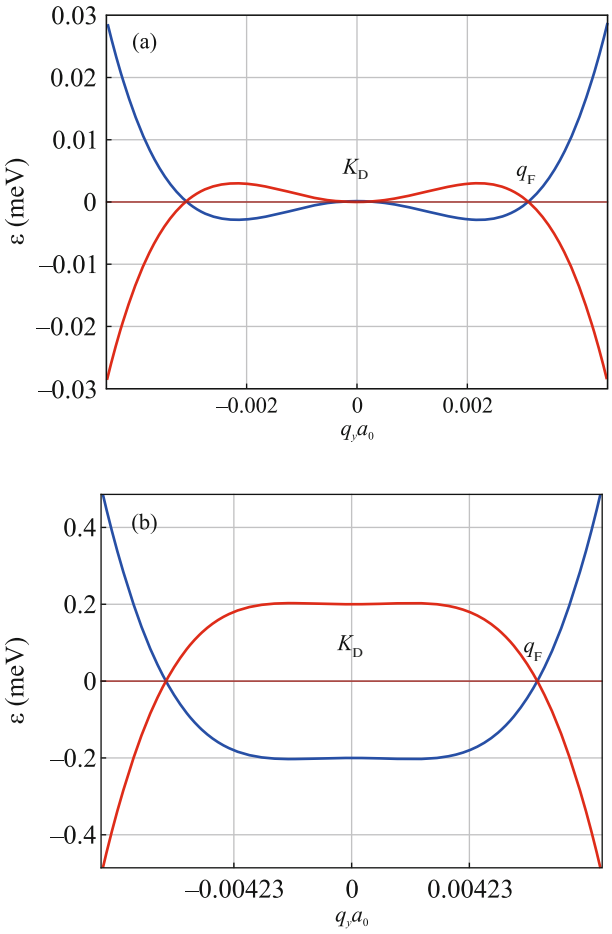

Fig. 3. (Color online) Dispersion curves of AB-stacked graphene deposited on a magnetic substrate (the $q_x = 0$ cut; q_y varies within a narrow range near the Dirac point K_D corresponding to $q_x = q_y = 0$) at $h = 11.6$ meV (200 T) and $\tilde{h}$ = (a) 0 and (b) 0.2 meV. The energy is measured from the Fermi level. The Fermi radius q_F is indicated. In panel (a), band touching occurs at the Dirac point. In panel (b), it is seen that even a small $\tilde{h}$ value gives rise to a sharp increase in the Fermi radius q_F and in the Fermi sea depth.

Let δ be the area of the region bounded by $\mathbf{q}_F$. Since this area is rather small, each connectivity component is approximated by a circle of a small radius q_F. The centers of these two circles coincide with the Dirac points K_D and K_D'. A low Fermi momentum q_F allows us to use the approximation $|f_{\mathbf{q}F}| \approx 3a_0 q_F/2$. First, we consider the case of $\tilde{h} = 0$. In this case, we find

$$q_F \approx \frac{2h}{3a_0 t}. \quad (9)$$

However, this formula becomes incorrect even at not-too-large $\tilde{h}$. Indeed, it is easy to demonstrate that the expression for the Fermi surface radius at $h \gg \tilde{h} \gg \frac{h^3}{t_0^2}$ takes the form

$$q_F \approx \frac{2}{3a_0 t}\sqrt{t_0\sqrt{h\tilde{h}}}. \quad (10)$$

Comparing this formula for q_F with Eq. (9), we find that even small $\tilde{h}$ significantly affects the Fermi radius.

The emerging Fermi surface is half-metallic since among four types of charge carriers (electrons and holes, each of them has two spin projections), only charge carriers of two types (electrons with spin $\sigma = -1$ and holes with spin $\sigma = +1$) reach the Fermi level.

The redistribution of charge carriers among the bands leads to the spin polarization of the graphene sample. Bands 4 and 5 forming the Fermi surface are characterized by the opposite values of σ; therefore, the redistribution of charge carriers from one band to the other is accompanied by the spin flip for each transferred charge carrier. The number of transferred charge carriers (per unit cell) is δ/S_{BZ}, where $\delta = 2\pi q_F^2$ and $S_{BZ} = 8\pi^2/(3\sqrt{3}a_0^2)$ is the Brillouin zone area for graphene. Each transferred electron contributes two $\hbar/2$ quanta to the total spin of the system; hence, the specific spin polarization in the $\tilde{h} = 0$ approximation is given by the expression

$$m = \frac{\hbar h^2}{\sqrt{3}\pi t^2}. \quad (11)$$

In the case of $h \gg \tilde{h} \gg \frac{h^3}{t_0^2}$, we have

$$m = \frac{\hbar t_0\sqrt{h\tilde{h}}}{\sqrt{3}\pi t^2}, \quad (12)$$

where Eq. (10) is used. We see that nonzero $\tilde{h}$ leads to a drastic increase in the magnetization.

Let us further generalize our model taking into account the nonequivalence of the layers due to both contact with the substrate and the applied dc electric field. We assume that the substrate creates a finite difference ϕ_0 in potential energies of the layers. In addition, we assume that the gate electrodes can generate the electric field E perpendicular to the sample plane. To include these effects into our formalism, we modify the matrix V_σ in Eq. (5) to the form

$$V_\sigma = \mathrm{diag}\left(\sigma h + \frac{\phi}{2}, \sigma h + \frac{\phi}{2}, \sigma\tilde{h} - \frac{\phi}{2}, \sigma\tilde{h} - \frac{\phi}{2}\right), \quad (13)$$

where

$$\phi = \phi_0 - eEd = -eE^*d. \quad (14)$$

Here, $E^* = E - \phi_0/(ed)$ is the effective field incorporating the combined effect of both the substrate and the electric field E on electrons in our system. The suggested model extends the approach employed in [10].

The band structure at finite h, $\tilde{h}$, and ϕ values is described by the formula

$$\varepsilon_{\mathbf{q}}^{(1,\ldots,8)} = \frac{\sigma(h+\tilde{h})}{2} + \chi\left[\frac{(\phi + \sigma(h-\tilde{h}))^2}{4} + |f_{\mathbf{q}}|^2t^2 + \frac{t_0^2}{2} + \kappa\sqrt{(\phi + \sigma(h-\tilde{h}))^2|f_{\mathbf{q}}|^2t^2 + |f_{\mathbf{q}}|^2t^2t_0^2 + \frac{t_0^4}{4}}\right]^{1/2}. \quad (15)$$

This expression generalizing Eq. (7) is used below to study the effect of the applied field on the system properties.

3. METAL–INSULATOR TRANSITION

It is well known that the electric field perpendicular to the AB-stacked graphene sample induces its transition to the insulating state. On the other hand, we show that bilayer AB-stacked graphene deposited on the ferromagnetic substrate is a metal in the $\phi = 0$ limit. Consequently, it is interesting to determine the minimum value of ϕ sufficient to open a gap in the spectrum of the system under study. A relatively simple analysis demonstrates that the system is metallic if bands 4 and 5 given by the expression

$$\varepsilon_{\mathbf{q}}^{(4,5)} = \pm\frac{h+\tilde{h}}{2} \mp \left[\frac{(\phi \pm (h-\tilde{h}))^2}{4} + |f_{\mathbf{q}}|^2t^2 + \frac{t_0^2}{2} - \sqrt{(\phi \pm (h-\tilde{h}))^2|f_{\mathbf{q}}|^2t^2 + |f_{\mathbf{q}}|^2t^2t_0^2 + \frac{t_0^4}{4}}\right]^{1/2} \quad (16)$$

overlap with each other. Otherwise, bilayer graphene is an insulator. Thus, the metal–insulator transition occurs when the top of band 4

$$\varepsilon_{\max}^{(4)} = \frac{h+\tilde{h}}{2} - \frac{t_0(h-\tilde{h}+\phi)}{2\sqrt{(h-\tilde{h}+\phi)^2 + t_0^2}} \quad (17)$$

coincides with the bottom of band 5

$$\varepsilon_{\min}^{(5)} = -\frac{h+\tilde{h}}{2} + \frac{t_0|h-\tilde{h}-\phi|}{2\sqrt{(h-\tilde{h}-\phi)^2 + t_0^2}}. \quad (18)$$

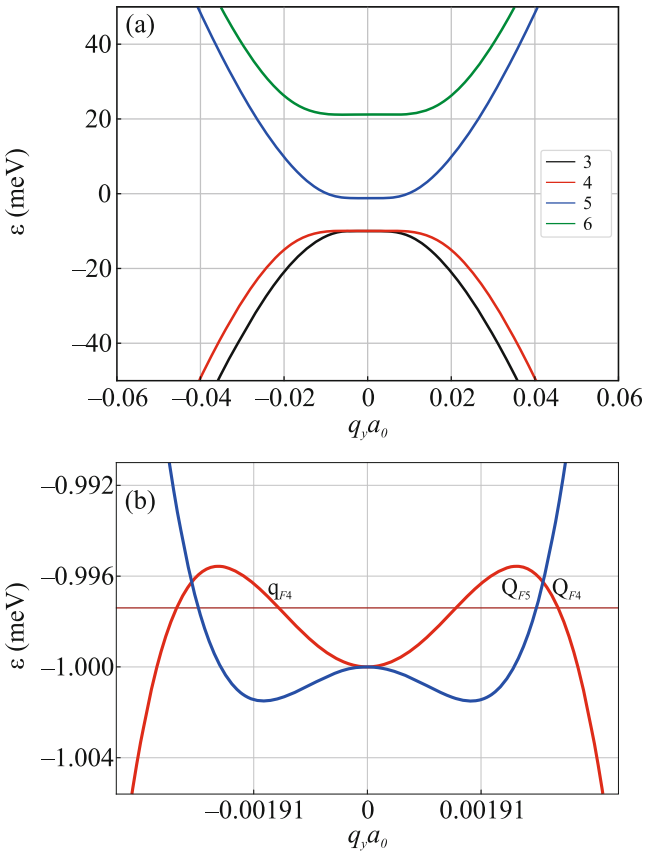

Fig. 4. (Color online) Dispersion curves near the Dirac point K_D of AB-stacked graphene deposited on a magnetic substrate in the applied electric field (the $q_x = 0$ cut; q_y varies within a narrow range near the Dirac point K_D corresponding to $q_x = q_y = 0$) at $\tilde{h} = 0$ and $h = 11.2$ meV (190 T), so that $\phi_c = 11.22$ meV. (a) Insulating phase, $\phi = 20$ meV. The spectrum clearly exhibits the band gap separating valence bands 3 and 4 from the conduction band. (b) Metallic phase, $\phi = 2$ meV. Bands 4 and 5 are presented by the red and blue lines, respectively. Bands 3 and 6 are outside of the energy window in panel (b). The Fermi level is denoted by the horizontal straight line. The crossing points of the bands with the Fermi level correspond to the Fermi surface. The Fermi momenta are denoted as Q_{F4}, Q_{F5}, and q_{F4}.

Equating $\varepsilon^{(4)}_{max}$ to $\varepsilon^{(5)}_{min}$, it is easy to demonstrate that the system under study is an insulator (semiconductor) if $\phi > \phi_c$; at $h, \phi \ll t_0$, the critical value ϕ_c is given by the formula

$$\phi_c \approx h + \tilde{h} + \frac{2h^3}{t_0^2} + \frac{2\tilde{h}^3}{t_0^2}. \qquad (19)$$

The analysis of (19) shows that the cubic corrections to ϕ_c at typical values of exchange fields as high as hundreds of tesla make a negligibly small contribution.

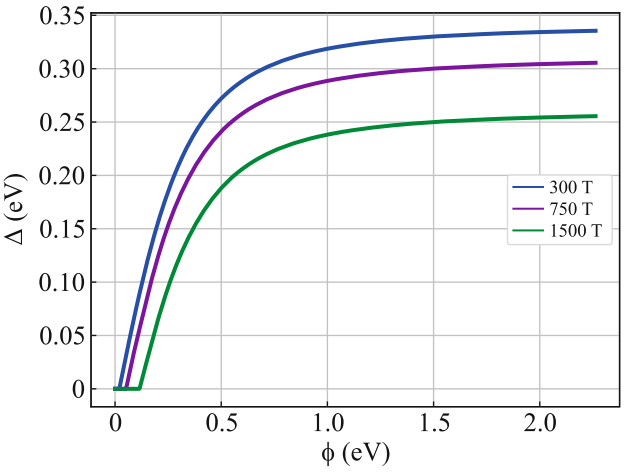

Fig. 5. (Color online) Band gap $\Delta = \Delta(\phi)$ at different exchanges field h and at $\tilde{h} = 0$. In the metallic phase ($\phi < \phi_c$), the gap vanishes. The plots demonstrate that the critical value ϕ_c increases with h; this agrees with Eq. (19).

Expressions (17) and (18) allow us to find the band gap $\Delta = \varepsilon^{(5)}_{min} - \varepsilon^{(4)}_{max}$,

$$\Delta = -h - \tilde{h} + \frac{t_0(\phi - h + \tilde{h})}{2\sqrt{(\phi - h + \tilde{h})^2 + t_0^2}} + \frac{t_0(\phi + h - \tilde{h})}{2\sqrt{(\phi + h - \tilde{h})^2 + t_0^2}}, \qquad (20)$$

see Fig. 4a. In the limit of very strong fields, $\phi \gg t_0$, Eq. (20) gives $\Delta \approx t_0 - h - \tilde{h}$. This asymptotic limit is clearly seen in Fig. 5, where we plot the function $\Delta = \Delta(\phi)$ at $\tilde{h} = 0$ and different Zeeman fields h. However, it would be quite difficult to create so wide band gaps in an actual experiment due to the possible electric breakdown of this heterostructure.

Note also that the spin polarization of the insulating phase is always absent, $m = 0$. Indeed, in the absence of the Fermi surface, the redistribution of charge carriers between the bands corresponding to opposite values of σ does not occur, and the number of electrons with the spin projection parallel to that of the field h is exactly equal to the number of electrons having the opposite spin projection.

Now, let us discuss the range $\phi < \phi_c$, where our system is metallic. A typical metallic spectrum is illustrated in Fig. 4b. In Section 2, we discussed the characteristics of the metallic state at zero effective field E^*. At nonzero h and ϕ values, the symmetry of Eqs. (8) is no longer valid; therefore, we cannon fix the Fermi level at $\varepsilon_F = 0$. It is necessary to consider the multicomponent Fermi surface determined by the standard condition $\varepsilon^{(4)}_{\mathbf{q}} = \varepsilon^{(5)}_{\mathbf{q}} = \varepsilon_F$. For band 4 at a positive ϕ value, these equations specify two concen-

tric circles centered at the point K_D. We denote the radii of these circles as q_{F4} and Q_{F4}, $q_{F4} < Q_{F4}$. The same situation takes place near the K_D' point. Band 5 contributes one more circle per each Dirac point. We denote their radius as Q_{F5}. Note that at $\phi = 0$, radii Q_{F5} and Q_{F4} coincide with each other and with q_F determined by Eq. (9), whereas radius q_{F4} vanishes. The arising Fermi surface should satisfy the condition

$$Q_{F4}^2 - q_{F4}^2 = Q_{F5}^2. \quad (21)$$

In other words, the number of states occupied by electrons in band 4 is equal to the number of empty states in band 5. At $\tilde{h} = 0$ and $\phi \ll h \ll t_0$, the problem can be explicitly solved:

$$\varepsilon_F \approx -\frac{\phi}{2} + \frac{4h^2\phi}{3t_0^2}. \quad (22)$$

At $\phi \to 0$, the derived relation shows that $\varepsilon_F = 0$ as is the case in zero effective field, see Section 2. Note also that the second term includes the ratio that is small in the typical physical situation: $h^2/t_0^2 \ll 1$. For example, at $h = 200$ T, the second term is three orders of magnitude smaller than the first one.

4. COMPARISON WITH THE COMPUTER SIMULATION RESULTS

To illustrate the usefulness of our approach, we compare our analytical calculations with the density functional theory [9]. Following [9], we define the "splittings" of the valence and conduction bands as follows

$$\lambda^{VB} = [\varepsilon_{\mathbf{q}}^{(4)} - \varepsilon_{\mathbf{q}}^{(3)}]_{\mathbf{q}=0} = h + \tilde{h} - \frac{|\phi + h - \tilde{h}|}{2} + \frac{|\phi - h + \tilde{h}|}{2}, \quad (23)$$

$$\lambda^{CB} = [\varepsilon_{\mathbf{q}}^{(6)} - \varepsilon_{\mathbf{q}}^{(5)}]_{\mathbf{q}=0} = h + \tilde{h} + \frac{|\phi + h - \tilde{h}|}{2} - \frac{|\phi - h + \tilde{h}|}{2}. \quad (24)$$

These two parameters characterize the "fine" structure of the spectrum and are easily calculated in our model.

The splittings λ^{VB} and λ^{CB} are interesting because Fig. 4b in [9] demonstrates how these parameters (and Δ) depend on the external electric field E_{ext} created by the gates. To plot λ^{VB}, λ^{CB}, and Δ as functions of E_{ext}, we should take into account that field E_{ext} generated by an external source (gates) is attenuated within the interlayer space of AB-stacked graphene due to the electron density redistribution between the layers. To this end, we introduce the permittivity ϵ of AB-stacked bilayer graphene and specify the following relation between ϕ and E_{ext}:

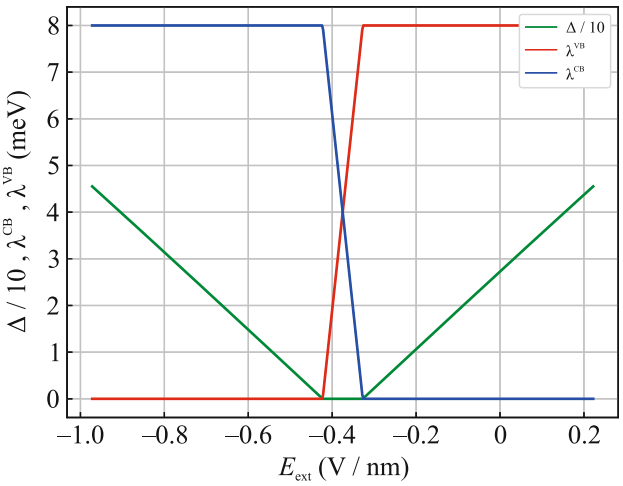

Fig. 6. (Color online) (Green line) Band gap $\Delta/10$ and the spin splitting of the (blue line) conduction and (red line) valence bands at $\tilde{h} = 0, h = 4$ meV, $\epsilon\phi_0/(ed) = -0.38$ V/nm, and $\epsilon = 4$ versus the external electric field E_{ext}. Note that a nonzero ϕ_0 value shifts the metallic phase to the $E \sim \epsilon\phi_0/(ed)$. The presented plots agree with Fig. 4b in [9].

$$\phi = \phi_0 - eE_{ext}d/\epsilon, \quad (25)$$

which corresponds to the substitution $E = E_{ext}/\epsilon$ in Eq. (14). The data presented in the top panel of Fig. 4 in [11] suggest that $\epsilon \sim 3.4$. Similar theoretical estimates can also be found in [12].

To determine the optimum values of parameters in our model, we analyzed Figs. 3 and 4 in [9]. In Fig. 3, one can notice that deep in the insulating phase, whose wavefunctions are predominantly localized in the upper layer, are nearly degenerate. This feature becomes possible at a very weak exchange field $\tilde{h}$ in the upper layer. Therefore, we chose $\tilde{h} = 0$. This allows us to reproduce an approximate degeneracy of the corresponding bands in the insulating phase, see Fig. 4a.

Figure 4b in [9] demonstrates that the splittings λ^{VB} and λ^{CB} in the insulating phase are saturated at about 8 meV. Analyzing Eq. (24) and (23), we can easily find that this behavior corresponds to $h = 4$ meV at $\tilde{h} = 0$. The choice of $\epsilon\phi_0/(ed) = -0.38$ meV provides the correct location of the metallic phase on the E_{ext} axis. Finally, we chose $\epsilon = 4$ to match the slopes of the $\Delta = \Delta(E_{ext})$ function in our formalism and in Fig. 4b in [9].

The corresponding plots are presented in Fig. 6. Our curves are in good agreement with Fig. 4b in [9] in both characteristic scales and qualitative behavior. In

other words, the choice of only four fitting parameters with a transparent physical meaning makes it possible to reproduce the dependences obtained as a result of the time-consuming numerical calculations.

5. DISCUSSION AND CONCLUSIONS

The most interesting feature of the heterostructure under study is the possibility to control its conductive properties by the gate voltage. The opening of a band gap in the perpendicular electric field applied to the AB-stacked graphene sample is a well-known theoretical result obtained in [13, 14] and confirmed experimentally in [11, 15–17]. We have generalized it to the case of a magnetic substrate. We have demonstrated that the magnetism of the substrate unexpectedly modifies the band structure of AB-stacked graphene. Indeed, instead of Fermi points with the parabolic dispersion relation near the touching of bands, which are destroyed at an arbitrarily small layer asymmetry ϕ, a nonzero h value induces a spin-polarized metal at small ϕ and an insulator at larger ϕ. Our simple model allows us to calculate the position of the metal–insulator transition and to study the properties of the phases on both sides of the transition.

Our calculations have demonstrated that the AB-bilayer graphene sample exhibits a nonzero magnetization m in the conducting phase. With an increase in ϕ, the system transforms to the insulating state with zero m; i.e., the magnetic characteristics of the heterostructure can be controlled by a nonmagnetic influence.

At zero ϕ, the electron and hole sheets of the Fermi surface of the system under study coincide with each other; i.e., nesting occurs. This feature of the band structure implies that the electron liquid at sufficiently low temperatures will be unstable with respect to the spontaneous nonsuperconducting ordering [18]. Deviation from $\phi = 0$ destroys nesting; therefore, ordering can be controlled by varying the gate voltage.

In addition, the conducting phase exhibits half-metallic characteristics: spins of the states on the electron (hole) Fermi surface sheet are perfectly polarized antiparallel (parallel) to the field h. This feature of the band structure could be used in the spin transport experiments.

In the insulating phase, the band gap can be rather wide: according to our estimate, $\Delta \sim t_0 - h - \tilde{h}$; i.e., it could be as high as several hundreds of meV. However, significant gap widths can require strong applied electric fields, and this increases the risk of the electric breakdown in the system as a whole.

In addition, in the wide gap limit, when $h \ll \phi \lesssim t_0$, magnetic phenomena can be less pronounced against the background of pure electrostatic ones. The $\phi \sim h$ regime seems more interesting since it is close to the metal–insulator transition. In this situation, to easily observe and/or utilize the discussed physical phenomena, substrates that can induce high fields h comparable to the energy corresponding to room temperature $T_r = 300$ K = 26 meV or even exceeding it are necessary. Otherwise, the usage of cryogenic technologies becomes inevitable.

To summarize, we have analytically studied AB-stacked bilayer graphene deposited on the insulating ferromagnetic substrate. The Hamiltonian of the model under study includes the exchange Zeeman and electrostatic fields, and also takes into account the asymmetry of the layers caused by contact with the substrate. In a low effective field, AB-stacked graphene is a metal, for which we have found a Fermi surface, which is half-metallic and can exhibit nesting. The sample itself has a nonzero spin polarization. When the critical electric field is exceeded, a gap opens in the spectrum of graphene. In the resulting insulating state, the total spin polarization vanishes. Our calculations are consistent with the density functional theory computer simulations. The possibility to control the gap together with nontrivial magnetic properties makes the heterostructure under discussion promising for spintronics applications.

FUNDING

This work was supported by the Russian Science Foundation (project no. 22-22-00464, https://rscf.ru/en/project/22-22-00464/).

CONFLICT OF INTEREST

The authors of this work declare that they have no conflicts of interest.

REFERENCES

1. W. Han, R. K. Kawakami, M. Gmitra, and J. Fabian, Nat. Nanotechnol. **9**, 794 (2014).
2. S. Roche, J. Åkerman, B. Beschoten, et al., 2D Mater. **2**, 030202 (2015).

3. S. S. Gregersen, S. R. Power, and A.-P. Jauho, Phys. Rev. B **95**, 121406(R) (2017).
4. K. S. Novoselov, A. K. Geim, S. V. Morozov, D. Jiang, Y. Zhang, S. V. Dubonos, I. V. Grigorieva, and A. A. Firsova, Science (Washington, DC, U. S.) **306**, 5696 (2004).
5. I. S. Sokolov, D. V. Averyanov, O. E. Parfenov, I. A. Karateev, A. N. Taldenkov, A. M. Tokmachev, and V. G. Storchak, Mater. Horiz. **7**, 1372 (2020).
6. A. V. Rozhkov, A. O. Sboychakov, A. L. Rakhmanov, and F. Nori, Phys. Rep. **648**, 1 (2016).
7. P. Wei, S. Lee, F. Lemaitre, L. Pinel, D. Cutaia, W. Cha, F. Katmis, Y. Zhu, D. Heiman, J. Hone, J. S. Moodera, and C.-T. Chen, Nat. Mater. **15**, 711 (2016).
8. K. Zollner, M. Gmitra, T. Frank, and J. Fabian, Phys. Rev. B **94**, 155441 (2016).
9. K. Zollner, M. Gmitra, and J. Fabian, New J. Phys. **20**, 073007 (2016).
10. P. Michetti, P. Recher, and G. Iannaccone, Nano Lett. **10**, 4463 (2010).
11. A. B. Kuzmenko, I. Crassee, D. van der Marel, P. Blake, and K. S. Novoselov, Phys. Rev. B **80**, 165406 (2009).
12. H. Min, B. Sahu, S. K. Banerjee, and A. H. MacDonald, Phys. Rev. B **75**, 155115 (2007).
13. E. McCann, Phys. Rev. B **74**, 161403(R) (2006).
14. E. McCann and V. I. Fal'ko, Phys. Rev. Lett. **96**, 086805 (2006).
15. E. A. Henriksen and J. P. Eisenstein, Phys. Rev. B **82**, 041412(R) (2010).
16. A. B. Kuzmenko, E. van Heumen, D. van der Marel, P. Lerch, P. Blake, K. S. Novoselov, and A. K. Geim, Phys. Rev. B **79**, 115441 (2009).
17. E. V. Castro, K. S. Novoselov, S. V. Morozov, N. M. R. Peres, J. M. B. Lopes dos Santos, J. Nilsson, F. Guinea, A. K. Geim, and A. H. Castro Neto, Phys. Rev. Lett. **99**, 216802 (2007).
18. D. N. Dresvyankin, A. V. Rozhkov, and A. O. Sboychakov, JETP Lett. **114**, 763 (2021).

Translated by K. Kugel